



# A palaeoecological model for the late Mesoproterozoic – early Neoproterozoic Atar/El Mreïti Group, Taoudeni Basin, Mauritania, northwestern Africa

Jérémie Beghin<sup>a,\*</sup>, Romain Guilbaud<sup>b</sup>, Simon W. Poulton<sup>c</sup>, Nur Gueneli<sup>d</sup>, Jochen J. Brocks<sup>d</sup>, Jean-Yves Storme<sup>a</sup>, Christian Blanpied<sup>e</sup>, Emmanuelle J. Javaux<sup>a,\*</sup>

<sup>a</sup> Department of Geology, UR GEOLOGY, University of Liège, Liège, Belgium

<sup>b</sup> Lancaster Environment Centre, Lancaster University, Lancaster LA1 4YQ, United Kingdom

<sup>c</sup> School of Earth and Environment, University of Leeds, Leeds LS2 9JT, United Kingdom

<sup>d</sup> Research School of Earth Sciences, The Australian National University, Canberra ACT 2601, Australia

<sup>e</sup> TOTAL, Projets Nouveaux, Paris, France

## ARTICLE INFO

### Keywords:

Palaeoredox conditions  
Iron speciation  
Early eukaryotes  
Palaeoecology

## ABSTRACT

Reconstructing the spatial distribution of early eukaryotes in palaeoenvironments through Proterozoic sedimentary basins provides important information about their palaeoecology and taphonomic conditions. Here, we combine the geological context and a reconstruction of palaeoenvironmental redox conditions (using iron speciation) with quantitative analysis of microfossil assemblages (eukaryotes and *incertae sedis*), to provide the first palaeoecological model for the Atar/El Mreïti Group of the Taoudeni Basin. Our model suggests that in the late Mesoproterozoic – early Neoproterozoic, the availability of both molecular oxygen and nutrients controlled eukaryotic diversity, higher in oxic shallow marginal marine environments, while coccoidal colonies and benthic microbial mats dominated respectively in anoxic iron-rich and euxinic waters during marine highstands or away from shore where eukaryotes are lower or absent.

## 1. Introduction

The mid-Proterozoic (~1.8–0.8 billion years ago) is often called ‘the boring billion’ mostly due to the relative stability of the carbon isotope record (Buick et al., 1995; Brasier and Lindsay, 1998) and little changes in atmospheric and ocean oxygen levels (e.g. Kah et al., 1999, 2004; Kah and Bartley, 2011 for review). However, the carbon isotope record changes from uniform early Mesoproterozoic (pre-1.3 Ga)  $\delta^{13}\text{C}_{\text{carb}}$  values of ~0‰, to mid-Mesoproterozoic (~1.3 to ~1.2 Ga) values between –0.5‰ and +2.0‰, to late Mesoproterozoic (~1.2 to ~1.0 Ga) values between –2.5‰ and +4.0‰. This implies changes in ocean chemistry, bioproductivity and tectonics, and may partly reflect progressive eukaryotic diversification (Kah et al., 1999; Bartley and Kah, 2004). Evidence of a more dynamic situation is now accumulating, in terms of tectonics (Roberts, 2013) with the formation and breakup of the supercontinents Nuna ~2.0–1.5 Ga ago (Evans, 2013) and Rodinia ~1.3–0.9 Ga ago (Karlstrom et al., 2001; Li et al., 2008; Johansson, 2014), redox conditions showing spatial and temporal heterogeneity (Poulton et al., 2010; Gilleaudeau and Kah, 2013b, 2015; Guilbaud et al., 2015), and patterns of biotic diversification (Knoll et al., 2006;

Javaux, 2011).

### 1.1. Mid-Proterozoic ocean

The mid-Proterozoic ocean is envisaged to have been characterized by ferruginous (anoxic and Fe-containing) deeper waters, euxinic (anoxic and sulphidic) mid-depth waters adjacent to productive continental margins, and oxygenated shallow waters (Poulton et al., 2010; Poulton and Canfield, 2011; Planavsky et al., 2011). Mid-Proterozoic eukaryotes would have found suitable ecological niches in nearshore environments as suggested by some bathymetric-dependent palaeoecological distributions of fossilized microbiota (Butterfield and Chandler, 1992; Buick and Knoll, 1999; Javaux et al., 2001; Javaux and Knoll, 2016).  $\text{N}_2$ -fixing photoautotrophic bacteria would have been favoured over eukaryotic algae where fixed-N was scarcer and/or sulphide impeding in the photic zone (Johnston et al., 2009; Gilleaudeau and Kah, 2013b). On the continental shelf, the balance between euxinic and ferruginous conditions may have been highly heterogenous in space and time after ~1.9 Ga (Poulton et al., 2010; Poulton and Canfield, 2011; Gilleaudeau and Kah, 2015; Planavsky et al., 2011). It

\* Corresponding authors at: Quartier Agora, Bâtiment B18, Allée du six août, 14, B-4000 Liège, Belgium.  
E-mail addresses: [jbeghin@ulg.ac.be](mailto:jbeghin@ulg.ac.be) (J. Beghin), [ej.javaux@ulg.ac.be](mailto:ej.javaux@ulg.ac.be) (E.J. Javaux).

<http://dx.doi.org/10.1016/j.precamres.2017.07.016>

Received 30 January 2017; Received in revised form 15 June 2017; Accepted 18 July 2017

Available online 19 July 2017

0301-9268/ © 2017 The Authors. Published by Elsevier B.V. This is an open access article under the CC BY-NC-ND license (<http://creativecommons.org/licenses/by-nc-nd/4.0/>).

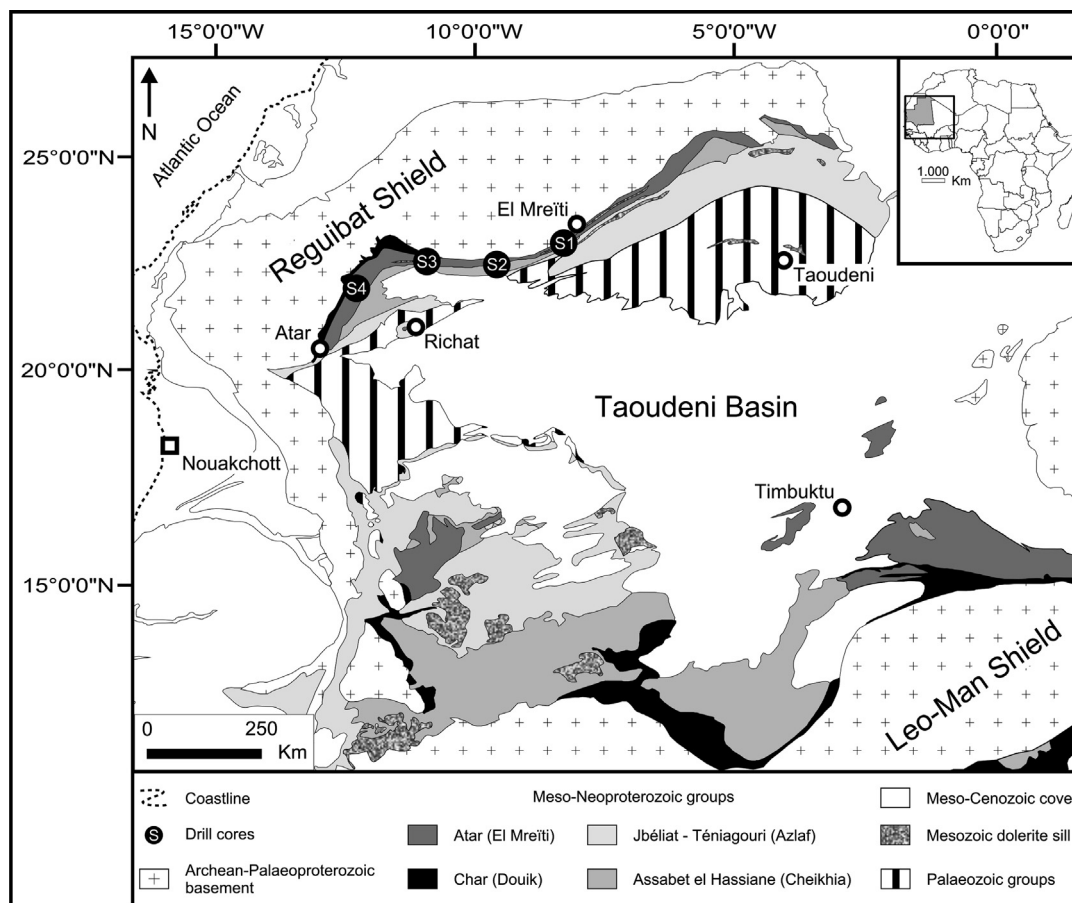


Fig. 1. Simplified geology of the Taoudeni Basin. Modified after Beghin et al. (2017) and modified from BEICIP (1981). Data from TOTAL (pers. comm., 2005). Locator map indicates Mauritania (in grey) in Africa and the studied area (rectangle) described on the main map.

was proposed that the extent of euxinic conditions may have hampered trace metal micronutrient availability, and Mo in particular would have been potentially limiting for N fixation in the mid-Proterozoic ocean (Anbar and Knoll, 2002; Gilleaudeau and Kah, 2013b). This in turn may have placed constraints on the nitrogen required for eukaryotic metabolisms, hence moderating eukaryote evolution (Anbar and Knoll, 2002). However, the mid-Proterozoic ocean was not globally euxinic but predominantly ferruginous (anoxic and  $\text{Fe}^{2+}$ -rich) in deep water environments with possible euxinia along continental margins (Poulton et al., 2010; Planavsky et al., 2011; Scott et al., 2013). Although the debate on low Mo limitations on N-fixation is still ongoing (e.g. Zerkle et al., 2006; Godfrey et al., 2013), and despite the relatively limited spatial extent of euxinia, Mo availability may have been low enough to limit N-fixation (Lyons et al., 2014). By contrast, the bioavailability of Zn, which is essential for a wide range of cellular functions, has been suggested to have been similar to modern levels and hence not limiting (Scott et al., 2013).

### 1.2. Pattern of early eukaryote diversification

Common explanations for the relatively moderate diversity of early eukaryotes in mid-Proterozoic oceans (Knoll et al., 2006; Javaux, 2011; Riedman et al., 2014; Cohen and MacDonald, 2015), following their Archean or Palaeoproterozoic origin and preceding their late Neoproterozoic increasing diversification, concern the widespread persistence of redox stratification in the ocean and related limitation of nutrients (Anbar and Knoll, 2002; Planavsky et al., 2011), and/or a low predation pressure by protists or animals (Butterfield, 2007, 2015; Porter, 2016; Javaux and Knoll, 2016). Although the interpretation of early eukaryotic microfossils as members of crown or stem groups may be

difficult, and despite possible sampling and preservation bias, a sharp increase in taxonomic richness (number of species) at the Ediacaran seems robust. The palaeoenvironmental conditions under which the first eukaryotic cells and associated metabolisms emerged are still unclear, although the evolution and diversification of early eukaryotes are generally linked to the availability of some molecular oxygen required to synthesize sterol in the cell membrane (Fenchel, 2012). Molecular and ultrastructural studies confirm that this is the case for crown group eukaryotes (Stairs et al., 2015). However, a growing body of work suggests that extensive oxygenation may not have been a requirement for the diversification of eukaryotes. Marine oxygen concentrations may have been high enough in local settings, perhaps close to cyanobacterial mats (Fischer, 1965; Hallmann and Summons, 2010; Kendall et al., 2010; Javaux, 2011; Knoll, 2014; Riding et al., 2014), and/or early eukaryotes may have been able to tolerate low marine oxygen concentrations (Butterfield, 2009; Javaux and Knoll, 2016). Stem eukaryotes may have originated and evolved in dysaerobic or subaerobic environments and could have been facultative anaerobic protists (Müller et al., 2012).

### 1.3. Purpose of this study

Here, we test the previously proposed hypotheses about the ecological distribution of eukaryotes in different depositional redox environments (e.g. Butterfield and Chandler, 1992; Buick and Knoll, 1999; Johnston et al., 2009; Javaux and Knoll, 2016), at the close of the late Meso – early Neoproterozoic, after the emergence of the firsts crown group eukaryotes and during the time period of their diversification (see Knoll, 2014; Butterfield, 2015; Cohen and MacDonald, 2015 for review). The late Mesoproterozoic – early Neoproterozoic Atar/El

Mreiti Group from the Taoudeni Basin, is known to bear exquisitely preserved microbial mats and organic-walled microfossils including unambiguous eukaryotes (Beghin et al., 2017).

## 2. Geological setting of the Taoudeni Basin

The Proterozoic and Phanerozoic strata of the Taoudeni Basin (Fig. 1) unconformably overlie an Archean-Palaeoproterozoic basement, the West African Craton (WAC), consisting of Mesoarchean (3.1–2.8 Ga) amphibolites and quartzo-feldspathic gneisses intruded by Palaeoproterozoic granitoids (2.0–2.2 Ga Eburnean Orogeny), and volcano-sedimentary deposits (Trompette and Carozzi, 1994; Villeneuve and Cornée, 1994; Lahondère et al., 2003; Schofield et al., 2006; Schofield and Gillespie, 2007). Since ca. 1.7 Ga, the basin has not experienced magmatic or major tectonic deformation, with the exception of the late Triassic opening of the North Atlantic Ocean (Clauer et al., 1982; Villeneuve and Cornée, 1994; Verati et al., 2005; Rooney et al., 2010). Proterozoic sedimentation started with tectonic reactivation of (NNE-SSW) basement normal faults during a phase of active extension (Benan and Deynoux, 1998; Rahmani et al., 2009). Horsts and grabens determined the lateral extent of the first Proterozoic deposits: the Char/Douik Group (Fig. 2) (Bronner et al., 1980; Benan and Deynoux, 1998). The overlying Atar/El Mreiti Group, studied here, was deposited unconformably on a tectonically stable craton and deposition ended with peneplanation across the WAC (Bertrand-Sarfati and Moussine-Pouchkine, 1988; Benan and Deynoux, 1998; Kah et al., 2012; Gilleaudeau and Kah, 2013a,b).

The type section for the Taoudeni Basin was previously described in

the Adrar region of the Mauritanian section (the Char and the Atar groups), in the western part of the basin (Trompette, 1973). Corresponding units at the northern central edge (Hank and Khatt areas) are respectively the Douik and the El Mreiti groups (Figs. 1 and 2). Most formations in the Atar/El Mreiti Group were constrained by a single age between  $890 \pm 35$  Ma, Unit I-5 and  $775 \pm 52$  Ma, Unit I-10 (Fig. 2). However, these Rb-Sr ages likely represent diagenetic mineralization possibly due to the Pan African collision (Rooney et al., 2010). The Atar/El Mreiti Group was dated at  $\sim 1.1$  Ga by Rooney et al. (2010) using Re/Os geochronology and at  $\sim 1.2$  Ga based on carbon isotope ( $\delta^{13}\text{C}_{\text{carb}}$ ) chemostratigraphy (Kah et al., 2009, 2012). The microfossil assemblage also confirmed a late Meso – early Neoproterozoic (Tonian) age (Beghin et al., 2017).

## 3. Material and methods

### 3.1. Sampling

Four cores were drilled on the northern margin of the Taoudeni Basin by Total S.A. in 2004 (Rooney et al., 2010). The cores were named from the east to the west, S1, S2, S3 and S4 (Fig. 1). S1 was not studied here because of contact metamorphism resulting from dolerite intrusions (Fig. 1). S2 was sampled ( $n = 143$ ) by E. J. Javaux in 2006 in Total laboratory and is described here in detail based on data from Total and personal observation of the core (Fig. 3 and Section 4.1). All S3 samples ( $n = 5$ ) come from the Aguel el Mabha Formation (laminated black and grey shale). Samples from S4 ( $n = 18$ ) come from the following three units: Unit I-3/Khatt Formation, Unit I-4/En Nesoar Formation and Unit I-5/Tourist and Aguel el Mabha formations; all S4 samples are dark grey or black shale. In core S2, we recognize five formations through the El Mreiti Group (Fig. 3), with two formations (En Nesoar and Tourist) chronostratigraphically constrained by Rooney et al. (2010) (Fig. 2, see also Beghin et al., 2017). According to previous studies (Kah et al., 2012; Gilleaudeau and Kah, 2013a,b, 2015), sediment of the El Mreiti Group (S2 core) was deposited under shallow water in an epicratonic (intra-cratonic) marine environment, while sediment of the Atar Group (S4 core) was deposited under shallow water in a pericratonic marine environment.

### 3.2. Redox reconstruction

Palaeoenvironmental and water column redox conditions were reconstructed using the iron speciation technique (Poulton and Canfield, 2005), whereby highly reactive iron ( $\text{Fe}_{\text{HR}}$ ), which includes carbonate-associated iron ( $\text{Fe}_{\text{carb}}$ ), ferric (oxyhydr)oxides ( $\text{Fe}_{\text{ox}}$ ), magnetite ( $\text{Fe}_{\text{mag}}$ ) and iron sulphides ( $\text{Fe}_{\text{py}}$ ), is quantified against total iron ( $\text{Fe}_{\text{T}}$ ). A total of 158 samples ( $S2 = 135$ ,  $S3 = 5$ ,  $S4 = 18$ ) were leached with Na-acetate, Na-dithionite, and ammonium oxalate to extract sequentially  $\text{Fe}_{\text{carb}}$ ,  $\text{Fe}_{\text{ox}}$ , and  $\text{Fe}_{\text{mag}}$ , respectively (Poulton and Canfield, 2005).  $\text{Fe}_{\text{py}}$  was determined by chromous chloride distillation (Canfield et al., 1986).  $\text{Fe}_{\text{T}}$  extractions were performed on ashed samples (8 h at  $450^\circ\text{C}$ ) using a  $\text{HNO}_3\text{-HF-HClO}_4$  digestion. Iron concentrations were measured by AAS, and replicate extractions gave a RSD of 8.97% ( $\text{Fe}_{\text{carb}}$ ), 3.28% ( $\text{Fe}_{\text{ox}}$ ), 6.68% ( $\text{Fe}_{\text{mag}}$ ), 4.58% ( $\text{Fe}_{\text{py}}$ ), and 3.44% ( $\text{Fe}_{\text{T}}$ ). Prior the calculation of highly reactive to total ( $\text{Fe}_{\text{HR}}/\text{Fe}_{\text{T}}$ ) and pyrite to highly reactive ( $\text{Fe}_{\text{py}}/\text{Fe}_{\text{HR}}$ ) iron ratios, the samples were screened to ensure sufficient total Fe, since low  $\text{Fe}_{\text{T}}$  carbonate-rich samples with  $\text{Fe}_{\text{T}} < 0.5$  wt% are not suitable for reconstructing redox conditions and can give erroneous results (Clarkson et al., 2014). Although carbonate-containing shale is dominant in the lower Aguel el Mabha Formation in S2,  $\text{Fe}_{\text{T}}$  was above this threshold for all the samples analyzed in this study.

The identification of water column anoxia via  $\text{Fe}_{\text{HR}}/\text{Fe}_{\text{T}}$  ratios is based on extensive calibration in modern (Canfield et al., 1986; Raiswell and Canfield, 1998; Poulton and Raiswell, 2002) and ancient (Raiswell et al., 2001; Poulton and Raiswell, 2002) marine settings. Sediments deposited under anoxic water columns are typically enriched

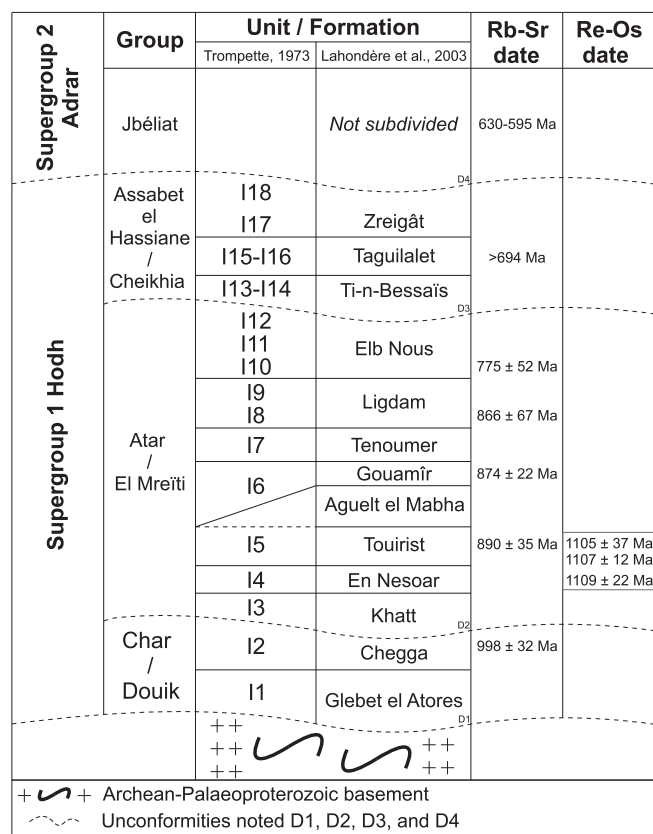


Fig. 2. Stratigraphy of Supergroups 1 (Hodh) and 2 (Adrar) of the Taoudeni Basin. Modified after Beghin et al. (2017) and modified after Rooney et al. (2010). Rb-Sr geochronology data from Clauer (1976, 1981), Clauer et al. (1982), Clauer and Deynoux (1987). Re-Os geochronology datings from Rooney et al. (2010). Stratigraphic nomenclature after Trompette (1973) and Lahondère et al. (2003). Sinusoidal dashed lines represent unconformities noted D1, D2, D3, and D4 (Lahondère et al., 2003). Linear dashed lines represent lateral changes.

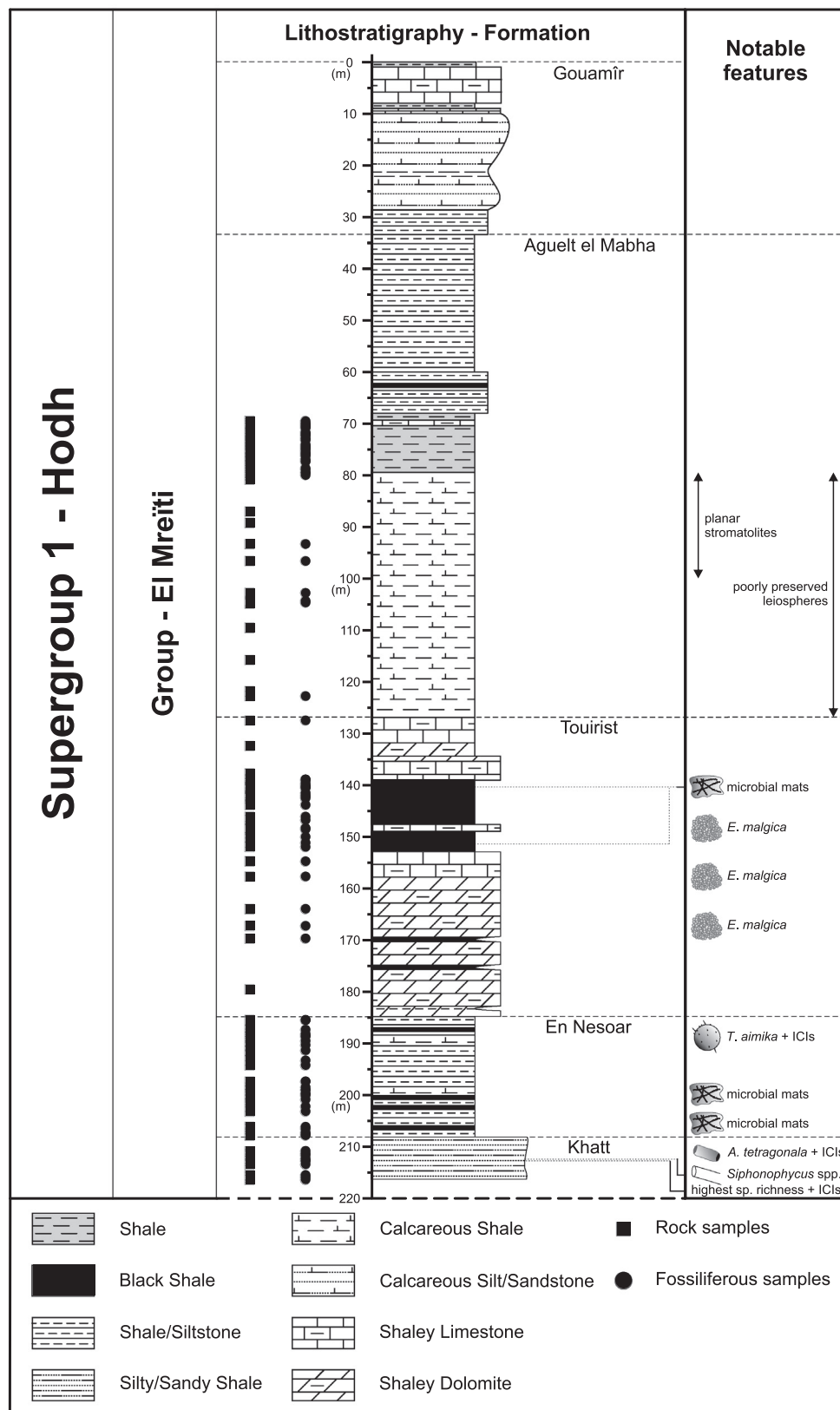


Fig. 3. Generalized lithostratigraphic column of the S2 core – El Mreiti Group (Supergroup 1 – Hodh), Taoudeni Basin, Mauritania modified after Beghin et al. (2017). Right column shows notable features ( $\geq 20\%$ , up to 95%, of relative abundance excepted for *Arctacellularia tetragonal* and *Siphonophycus* spp. which are  $\geq 5\%$ ; relative abundance of microfossil specimens is calculated without the total number of microbial mats; ubiquitous genera such as *Leiosphaeridia* and *Synsphaeridium* are not represented). Quantitative data detailed in Supplementary Table 2. See also Fig. 10. 'ICIs' represents horizons bearing numerous specimens showing inner opaque organic inclusions or intracellular inclusions.

in  $Fe_{HR}$ , resulting in  $Fe_{HR}/Fe_T \geq 0.38$  (Poulton and Canfield, 2011). By contrast, sediments deposited under oxic water column conditions are depleted in those minerals, resulting in  $Fe_{HR}/Fe_T \leq 0.22$  (Poulton and Canfield, 2011). Values between these values are considered equivocal

(Poulton and Canfield, 2011), and may represent anoxic deposition where the water column enrichment of  $Fe_{HR}$  has been masked by rapid sedimentation, or where some unsulfidized  $Fe_{HR}$  has been converted to Fe-rich sheet silicates during early diagenesis (Poulton and Raiswell,

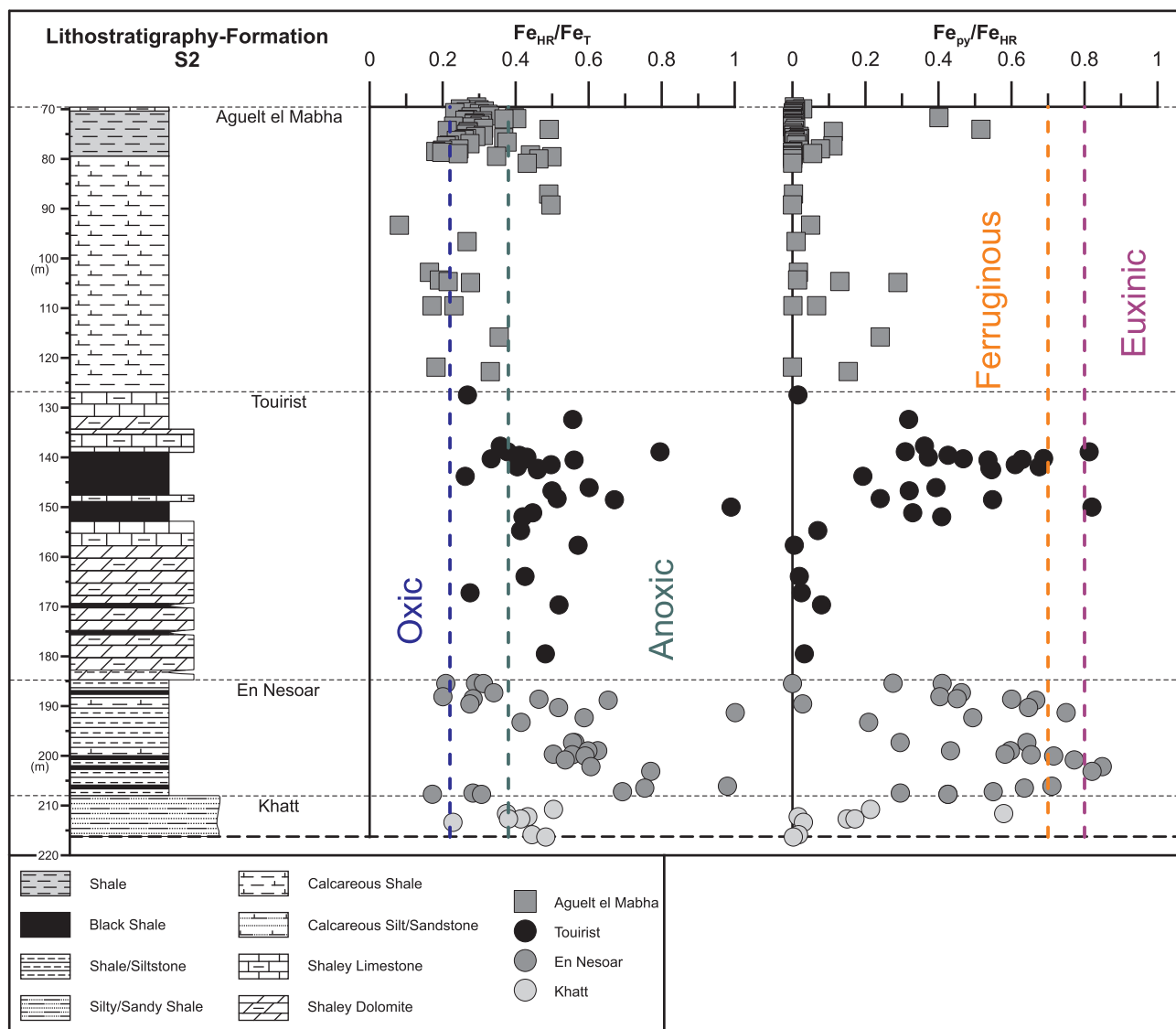


Fig. 4. Generalized lithostratigraphic column of the S2 core – El Mreiti Group (Supergroup 1 – Hodh), Taoudeni Basin, Mauritania modified after Beghin et al. (2017). Iron speciation data of S2:  $Fe_{HR}/Fe_T$  and  $Fe_{Py}/Fe_{HR}$ .

2002; Poulton et al., 2010; Cumming et al., 2013). For samples that were clearly deposited from anoxic bottom waters, the extent of pyritization of the highly reactive Fe pool can be used to distinguish euxinic ( $Fe_{Py}/Fe_{HR} \geq 0.8$ ) from ferruginous ( $Fe_{Py}/Fe_{HR} \leq 0.7$ ) water column conditions (Poulton et al., 2004; Poulton and Canfield, 2011). These ratios are used to reconstruct the average chemical composition of bottom waters, over the time interval represented by a sample, from the sediment-water interface up to the bottom of the chemocline, which may vary in depth.

### 3.3. Microfossil analyses

Of the 166 samples previously studied for microfossil diversity (Beghin et al., 2017), a total of 61 samples (S2 = 47, S3 = 5, S4 = 9) were analyzed quantitatively. A sample set was defined for each core, based on distinct lithofacies and palynofacies for each formation, with the aim of covering all the rock record diversity (Beghin et al., 2017) and to avoid any statistical bias. A statistical threshold of minimum 300 organic-walled microfossils (e.g. Moore et al., 1991; Jansonius and McGregor, 1996) to be counted per samples was defined (including acritarchs, multicellular forms, and filamentous forms). The counting was ended when a plateau of taxonomic richness was reached (i.e. the

number of species did not increase anymore with the number of specimens counted). The statistical threshold was not reached for 4 samples in S2, because of a very low occurrence of microfossils, and 11 samples in S2 were barren (Fig. 3). In other cases, more than 300 specimens were counted to reach the plateau. The biological affinities considered in this study were previously discussed in Beghin et al. (2017) and summarized in Supplementary Table 1. The diversity is reflected both by the species richness and the relative abundance. The species richness (S) is the total number of species observed in a sample. The relative abundance (%) is the total number of specimens counted for a selected species (noted n) or a group of species (e.g. eukaryotes or *incertae sedis*) in a sample, divided by the total number of all the specimens, whatever the species, counted in this sample (noted N) and multiplied by 100. The Simpson's Index of Diversity (1 - D) is calculated based on the Simpson's Index (D). The Simpson's Index is calculated following the formula:  $D = \sum \left(\frac{n}{N}\right)^2$ , with n and N as defined above. The value of the Simpson's Index of Diversity (1 - D) ranges between 0 and 1, and the higher the values indicating a greater sample diversity (see Supplementary Table 2).

## 4. Results

### 4.1. Description of the S2 core (El Mreïti Group)

The Khatt Formation (216.2–208.2 m) mainly consists of grey, green and brown silty to sandy shale interbedded with medium-grained sandstone (Fig. 3); with some occurrences of glauconite and pyrite. Abundant cross-bedding (hummocks, ripples, and waves) and gutter casts were observed. The En Nesoar Formation (208.2 to 184.72–80 m) mainly consists of grey, green and brown (rarely red, sometimes carbonate-containing) shale and laminated clayey siltstone interbedded with organic-rich layers or black shale, which are commonly pyritized (TOC values, at the bottom, from 2.1 to 13.6 wt%, Rooney et al., 2010). Occasional ripples, gutter casts and wavy bedding were also noted. The Tourist Formation (184.72–80 to 126.80 m) mainly consists of fine wavy light-grey to dark-grey laminated clayey dolomite or limestone, interbedded with fine layers of green clay and decimeter to meter thick finely laminated black shale (TOC values from 4.88 to 22.6 wt%, Rooney et al., 2010). The uppermost black shale of the Tourist Formation recorded some local slumps. The top of the Tourist Formation contains light-grey planar and wavy laminated carbonate and greyish green shaly carbonate (Fig. 3). The Aguelt el Mabha Formation (126.80–33.40 m) is mainly characterized by red or wine-coloured, brown and green carbonate-containing shale or clayey limestone, mudstone and very fine-grained siltstone (Fig. 3). Gutter casts and ripples were abundant in the middle part of this formation (~100–80 m) where red or wine-coloured carbonate-containing shale with thin lenticular calcareous bodies or planar stromatolites were observed. The Gouamîr Formation (33.40 m to the top) consists mainly of interbedded laminated carbonate-containing green silty shale and fine siltstone or grainstone and preserves lenticular bedding, ripples, hummocky cross-stratification, gutter casts, discrete micro slumps and wavy-bedding. The upper part (~10 m) of the Gouamîr Formation shows bright-white massively bedded carbonates.

### 4.2. Iron speciation

Shale from the Khatt Formation (S2) has  $Fe_{HR}/Fe_T$  above 0.22, with all but two samples being above 0.38 (mean = 0.41,  $n = 8$ ). The ratio of  $Fe_{py}/Fe_{HR}$  is more variable but all samples are below 0.60 (Fig. 4). The ratios of both  $Fe_{HR}/Fe_T$  and  $Fe_{py}/Fe_{HR}$  are highly variable in the En Nesoar Formation (0.17–1.0 and 0.0–0.85, respectively).  $Fe_{HR}/Fe_T$  is commonly > 0.38 in the Tourist Formation, with some samples falling between 0.22 and 0.38 (range = 0.26–0.99; Fig. 4), while  $Fe_{py}/Fe_{HR}$  is highly variable (0.01–0.82). In more detail, green shale at the base of the Tourist Formation (~185–155 m depth) has low  $Fe_{py}/Fe_{HR}$  ratios (< 0.08), while black shale from the upper part (~140–155 m depth) tends to have higher, but variable,  $Fe_{py}/Fe_{HR}$  ratios, with two samples above 0.8 (Fig. 4). Shale from the Aguelt el Mabha Formation (S2) has  $Fe_{HR}/Fe_T$  ratios < 0.38 (with some < 0.22) in the lower section, while upper section shows a spread from < 0.22 to > 0.38 (Fig. 4). The ratio of  $Fe_{py}/Fe_{HR}$  tends to be low, with a few samples having higher ratios (up to a maximum of 0.55).

For core S3, only limited samples were available. Five samples from the Aguelt el Mabha Formation were analyzed, giving intermediate  $Fe_{HR}/Fe_T$  ratios of 0.25–0.34 (mean = 0.29), while ratios of  $Fe_{py}/Fe_{HR}$  were very low (0.0) for each sample (not illustrated, see Supplementary Table 3).

In core S4,  $Fe_{HR}/Fe_T$  ratios for units I-3 and I-4 are consistently well above 0.38 with  $Fe_{py}/Fe_{HR}$  ratios that vary between 0.47 and 0.9 (Fig. 5). For Unit I-5 (S4)  $Fe_{HR}/Fe_T$  ratios are significantly lower (between 0.12 and 0.55, but mostly at the lower end) while  $Fe_{py}/Fe_{HR}$  ratios are also lower (< 0.47).

### 4.3. Quantitative microfossils analysis

The El Mreïti Group (S2) reveals a decreasing trend in total species richness, from the Khatt Formation to the top of the Tourist Formation (Fig. 6; Supplementary Table 2). The Khatt Formation records the highest total species richness ( $S = 32$ ) at 212.66 m depth (green shale). The Khatt assemblage, in addition to ubiquitous species such as *Leiosphaeridia* spp., *Obruchevella* spp., and *Siphonophycus* spp. (see Beghin et al., 2017), is mainly comprised of filamentous (*Arctacellularia tetragonala*) and coccoidal colonies (*Eomicrocystis malgica*, *Ostiana microcystis* and *Synsphaeridium* spp.), pseudoseptate unbranched filamentous sheath (*Tortunema wernadskii*), and botuliform vesicles (*Navifusa majensis* and several morphotypes of *Jacutianema solubila*). At the transition between the Khatt and En Nesoar formations (black shale), the total species richness decreases to 5–9, and then increases to 20 species at the top of En Nesoar (green shale) at 188.6 m depth. The En Nesoar assemblage, in addition to ubiquitous species such as *Leiosphaeridia* spp., *Obruchevella* spp., *Siphonophycus* spp., and *Synsphaeridium* spp., is mainly composed, at the base, of pyritized microbial mats with iron sulphide grains infilling filamentous sheaths and, at the top, by relatively large (> 70  $\mu\text{m}$  in diameter) spheroidal vesicles (*Leiosphaeridia tenuissima* and *L. jacutica*) and abundant large process-bearing acritarchs (*Trachyhystrichosphaera aimika*, up to 2–25% of the assemblage, and *T. botula*). The Tourist Formation (black and carbonate-containing green shale) records a lower total species richness to 5–9. The Tourist assemblage, in addition to ubiquitous species such as *Leiosphaeridia* spp., *Siphonophycus* spp. and *Synsphaeridium* spp., is dominated, in the middle part, by *Eomicrocystis malgica* (25–95%) and, in the upper part, by microbial mats with pyritized filamentous sheaths (25–35%). No microfossils were observed at the top of the Tourist Formation (carbonate-containing green shale and light-grey carbonate) and in the lower part of the Aguelt el Mabha Formation (carbonate-containing red shale with lenticular bodies), with the exception of three samples (2–3 species, mainly poorly preserved very thin-walled spheroidal vesicles) at the base of the Aguelt el Mabha Formation (at 122.78 m, 79.59 m and 80.03 m depth). The green shaly section of the Aguelt el Mabha Formation (70–80 m depth) records a new increase in the total species richness (9–11 species) dominated by ubiquitous species such as *Leiosphaeridia* spp., *Siphonophycus* spp. and *Synsphaeridium* spp. The Aguelt el Mabha Formation (5 samples of grey shale) from the S3 core also records a maximum of 11 species (at 123.37 m and 61.27 m depth) and, in addition to ubiquitous species such as *Leiosphaeridia* spp., *Siphonophycus* spp., and *Synsphaeridium* spp., is mainly composed of *Leiosphaeridia kulgunica* (spheroidal vesicles with a circular opening: a pylome interpreted as an excystment structure), *L. crassa* (showing a medial split also interpreted as an excystment structure), spheroidal vesicles including another vesicle (*Pterospermopsimorpha insolita*), and to a lesser extent of botuliform vesicles (*Navifusa majensis*) (see Supplementary Table 2).

The Atar Group (S4) shows a total species richness which is moderately high and steady throughout the core (units I-3, I-4, and I-5; dark-grey or black shale), from 10 to 21 species (Fig. 7). The Atar Group assemblage, in addition to ubiquitous species such as *Leiosphaeridia* spp., *Siphonophycus* spp. and *Synsphaeridium* spp. which are present through the core, is mainly composed at the base (units I-3 and I-4) of *Arctacellularia tetragonala*, *Chlorogloeaopsis* spp., several morphotypes of *Jacutianema solubila*, and *Navifusa majensis* and at the upper part (units I-4 and I-5), of *Arctacellularia tetragonala*, *Obruchevella* spp. and *Tortunema* spp. (Supplementary Table 2). Regarding the occurrence of the following eukaryotes and *incertae sedis*, three morphotypes of *Jacutianema solubila*, *Chlorogloeaopsis contexta* and *Tortunema* spp. and also some dominant species, Unit I-3 and to a lesser extent I-4 show similarities in the assemblage composition with the coeval epicratonic Khatt Formation (Supplementary Table 2).

Inner opaque organic inclusions (spheroidal or elongate) were numerously observed in several specimens, especially in three distinct

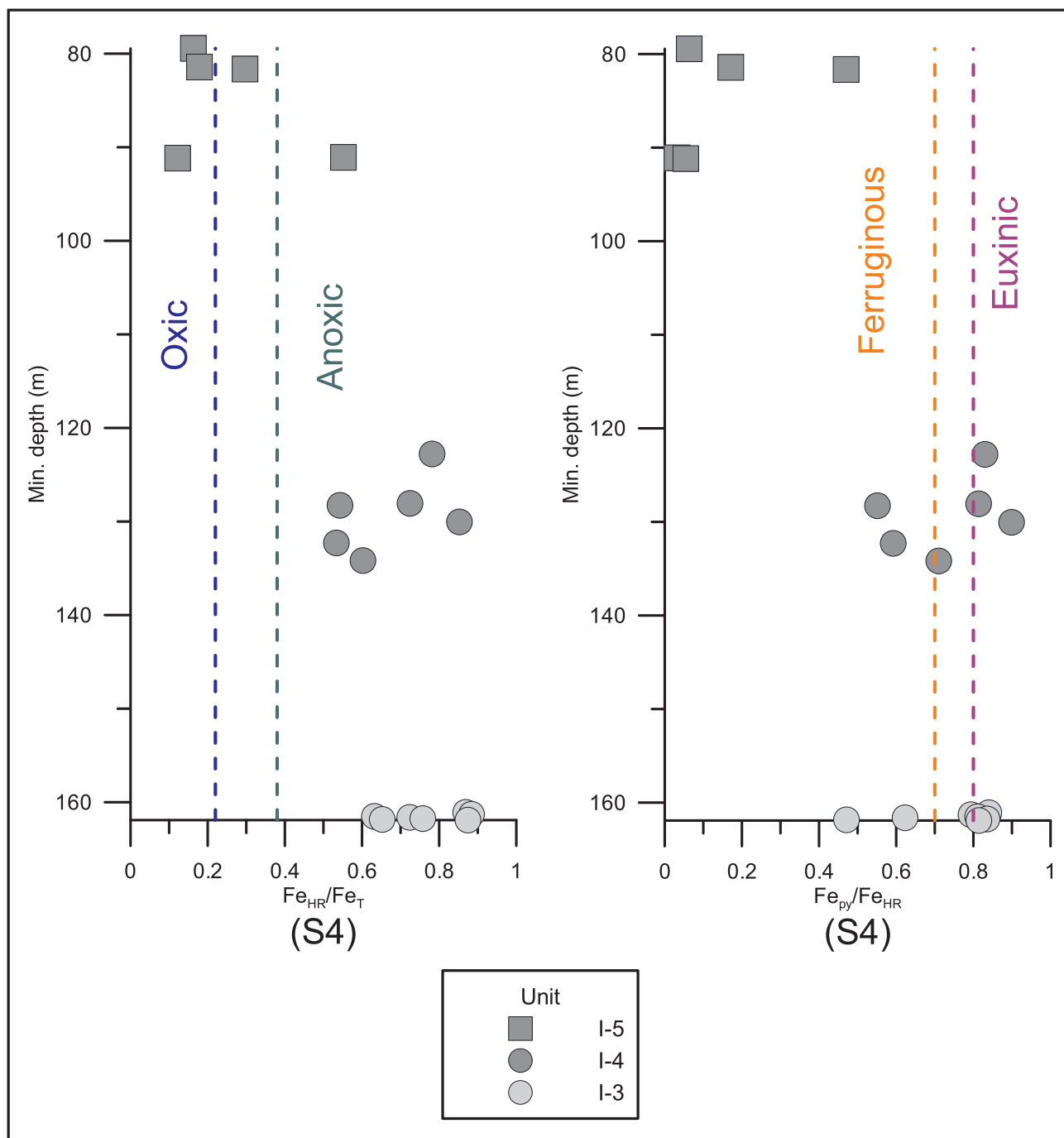


Fig. 5. Iron speciation data of S4:  $Fe_{HR}/Fe_T$  and  $Fe_{Py}/Fe_{HR}$ .

horizons of the S2 core at 212.66–77 m and 211.24 m (1–2% of specimens, mainly *A. tetragonala*) and 188.6 m (~5% of specimens, mainly *T. aimika*) depth (see Fig. 3: intracellular inclusions or ICIs), where preservation is exquisite.

## 5. Discussion

### 5.1. Marine sedimentary depositional environments (El Mreiti Group)

The El Mreiti Group is defined by several sedimentary depositional environments (Lahondère et al. 2003; Kah et al., 2012; Gilleaudeau and Kah, 2013a,b, 2015). The Khatt Formation was deposited in facies ranging from fluvial-deltaic to marine tidal-flat to shallow marine (Kah et al., 2012), with occasional tempestites (Lahondère et al., 2003). The

En Nesoar Formation comprises shallow subtidal marine sediments deposited during a marine transgression (Kah et al., 2012) or during subsidence when compared to the underlying Khatt Formation (Lahondère et al., 2003). Sediment from the S2 core likely indicate deposition of the En Nesoar Formation under lower energy than the Khatt Formation and under higher energy than the Tourist Formation, as also suggested by the presence of columnar (*Tungussia* sp. or *Inzeria* sp.) stromatolites reported by Lahondère et al. (2003) and Kah et al. (2012). The Tourist Formation is interpreted as a predominantly shallow-marine environment deposited under the fair-weather wave base (Kah et al., 2012; Gilleaudeau and Kah, 2013a) during the most extensive flooding of the WAC (Gilleaudeau and Kah, 2013a). Moreover, coniform (*Conophyton-Jacutophyton* sp.) stromatolites of the Tourist Formation (Lahondère et al., 2003; Kah et al., 2012) or Unit-I5

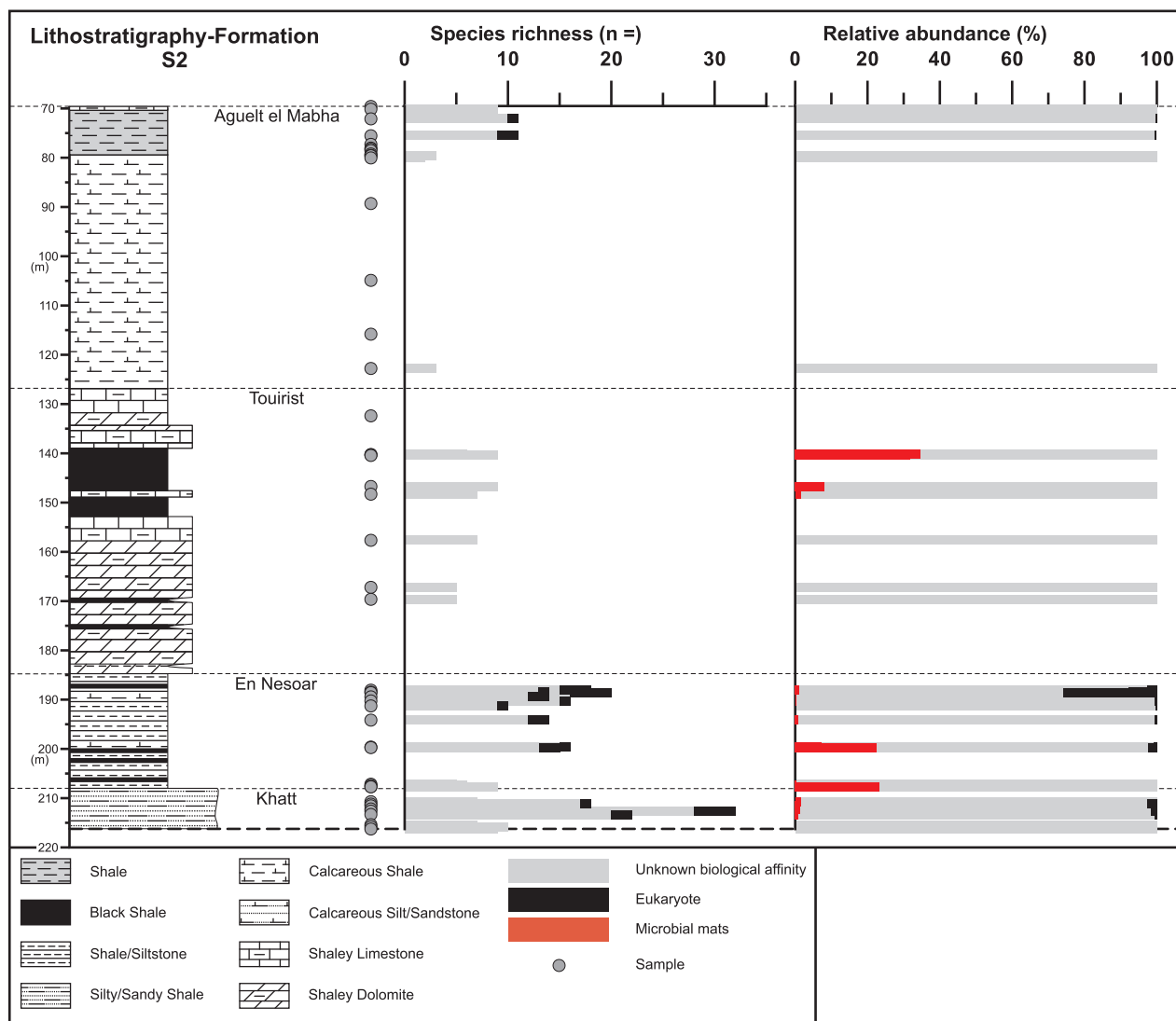


Fig. 6. Generalized lithostratigraphic column of the S2 core – El Mreiti Group (Supergroup 1 – Hodh), Taoudeni Basin, Mauritania modified after Beghin et al. (2017). Quantitative microfossils analysis of S2: species richness (n =) and relative abundance (%) of unambiguous eukaryotes and microfossils of an unknown biological affinity (*incertae sedis*). Relative abundance of microfossil specimens is calculated without the total number of microbial mats. Microbial mats are not counted in the total species richness. Relative abundance of microbial mats is calculated separately (see Supplementary Table 2).

(Kah et al., 2009, 2012) suggest a deeper (lower energy but still in the photic zone) depositional environment during marine highstands with little or no sediment influx compared to the En Nesoar Formation. The overlying Aguel el Mabha Formation, according to Kah et al. (2012), represents a more proximal facies (planar stromatolites, this study), where shallow-marine carbonate records increasing siliciclastic sedimentation (Fig. 3), which contrasts with earlier models interpreting this formation as being an inter-stromatolitic deposit (Bertrand-Sarfati and Moussine-Pouchkine, 1992). These shallow-water facies would have been deposited after a major regression which may have occurred at the transition (see Fig. 3, carbonates at 135 m depth) from the Tourist to Aguel el Mabha Formation (Kah et al., 2012; Gilleaudeau and Kah, 2013a). The Aguel el Mabha Formation shows characteristics of restricted environments (inner shelf basins) in an epicratonic setting suggesting a complex palaeogeography (Lahondère et al., 2003; Gilleaudeau and Kah, 2013a).

5.2. Palaeoredox reconstruction

The dominantly anoxic ferruginous signal of the Khatt Formation (Fig. 4), with two samples being equivocal, is not expected for this

environment with high wave energy (interpreted as fluvial-deltaic to marine tidal-flat). This formation should rather display an oxic signal. The Taoudeni Basin has not suffered significant post-depositional metamorphism away from the contact areas with mafic intrusions (Rooney et al., 2010; Gilleaudeau and Kah, 2013b, 2015), but Gilleaudeau and Kah (2013a) reported intense secondary mineralization in the Khatt Formation resulting from diagenetic fluids. This may have altered the geochemical signals making them difficult to interpret. However, there is no evidence of hydrothermal circulation or alteration in our rock material. Diagenetic remobilization of Fe between the non-sulfidic Fe<sub>HR</sub> pools is expected but would not change much the primary signal. Late sulfidation is probably negligible as little or no acid volatile sulphide (AVS) was extracted during lab procedure. The excellent preservation state of organic-walled microfossils in these samples suggests that the primary signal is not influenced by secondary oxidation. The ferruginous signal of the Khatt Formation is here probably a primary signature. In such proximal environments (Khatt Formation), local enrichments in highly reactive iron (due to the proximity to the source), without invoking or requiring anoxia, have to be taken into consideration. However, this is speculative as the level of description of the Khatt Formation is limited by the absence of marker beds. The majority

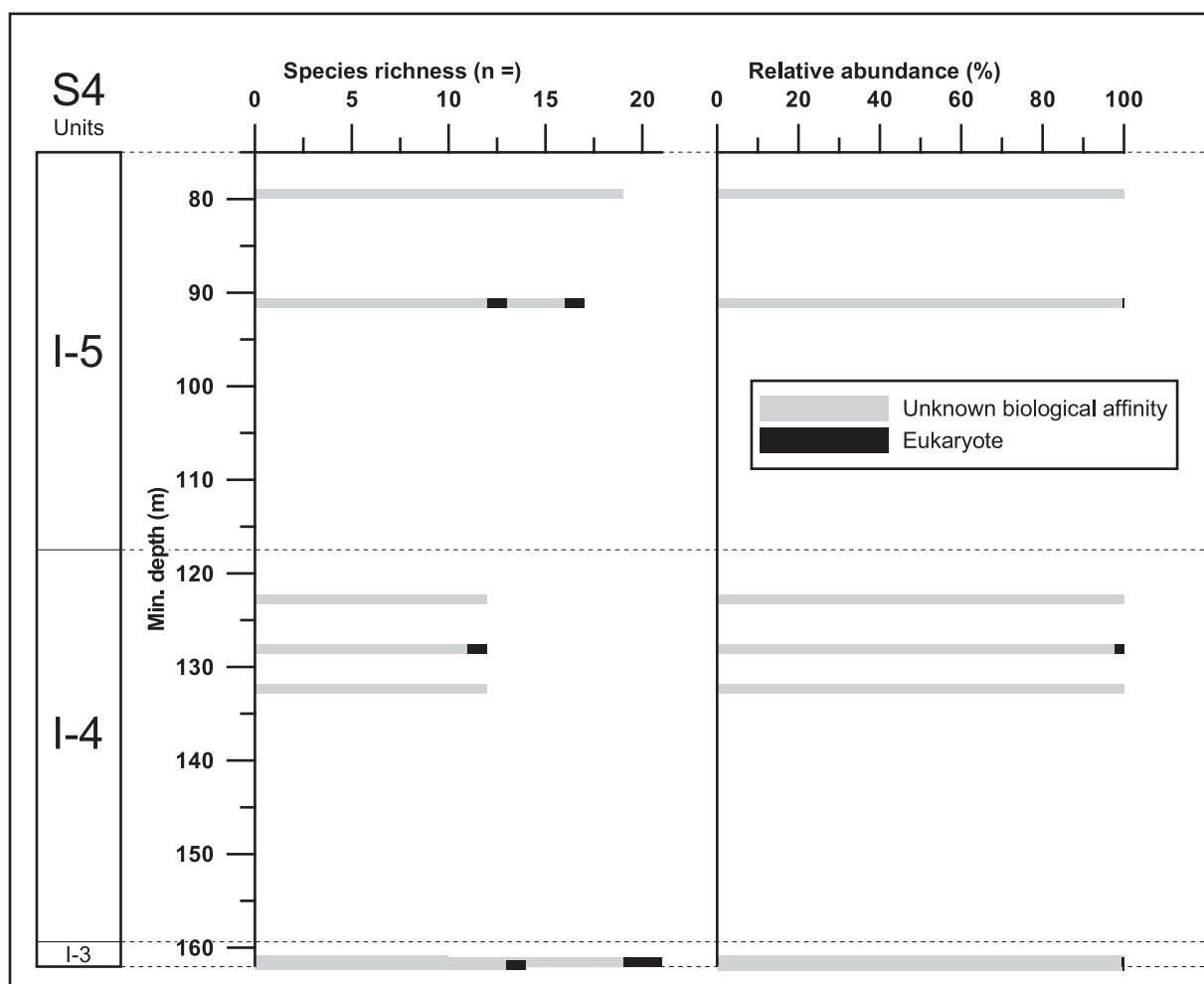


Fig. 7. Quantitative microfossils analysis of S4: species richness ( $n =$ ) and relative abundance (%) of eukaryotes and microfossils of an unknown biological affinity. Atar Group units on the left side.

of samples of the En Nesoar Formation indicate anoxic deposition, with fewer samples that give an equivocal or oxic signal. Many of the anoxic samples have relatively low  $Fe_{py}/Fe_{HR}$ , indicating ferruginous conditions, but with some suggestion for the development of bottom water euxinia, particularly in the lower portion of the formation (Fig. 4). During the most extensive flooding of the WAC, the Tourist Formation also records dominantly anoxic ferruginous conditions, with possible occasional euxinia (Fig. 4); while Gilleaudeau and Kah (2015) reported both oxic and anoxic but mainly euxinic conditions. After the major regression at the transition between the Tourist and Aguel el Mabha Formations (~135 m depth), the Aguel el Mabha Formation records both oxic and anoxic and iron-rich conditions, but with many samples being equivocal (Fig. 4). Oxic conditions in the Aguel el Mabha Formation (S2 core) are more clearly prevalent at the base (carbonate-containing shale), with the lowest  $Fe_{HR}/Fe_T$  ratio of 0.08 recorded in a sample where thin lenticular calcareous beds and/or planar stromatolites were observed (red carbonate-containing shale, 80–100 m depth). Similar to many of the samples in core S2 (Aguel el Mabha Formation), Fe speciation data were equivocal for core S3 (Supplementary Table 3).

Data for the pericratonic Atar units I-3 and I-4 suggest anoxic conditions, both ferruginous and euxinic, while Unit I-5 records both oxic and anoxic iron-rich deposition. Euxinia is relatively more prevalent in units I-3 and I-4 than in their coeval epicratonic strata (Khatt and En Nesoar formations; Figs. 4, 5 and 8; Supplementary Table 3).

Gilleaudeau and Kah (2015) recently provided a detailed study of palaeoredox conditions in the Taoudeni Basin using Fe-speciation. This study confirms that the Khatt and Aguel el Mabha formations, S2 and

S3 cores, called 'Environment I' by Gilleaudeau and Kah (2015), were suggested to reflect dominantly oxic or anoxic iron-rich conditions, which is supported by our data (Fig. 4). The En Nesoar and Tourist formations, referred to as 'Environment II' by Gilleaudeau and Kah (2015), were reported to indicate fluctuating oxic to euxinic bottom waters; our findings also support this interpretation (Fig. 4). However, we find no evidence for oxic depositional conditions in the Tourist Formation. This may be linked to lithological differences in the samples studied by Gilleaudeau and Kah (2015), which were mainly restricted to black shale, albeit with a slightly lower TOC (0.4–15.3 wt%) than the En Nesoar and Tourist Formations studied here (2.06–22.56 wt%; Rooney et al., 2010). These differences reflect highly heterogeneous depositional redox conditions, as previously suggested by Gilleaudeau and Kah (2013a), and could be related to heterogeneous input sources in space and time across the Taoudeni Basin (complex palaeogeography on the craton interior) and/or fluctuating redox conditions during early anoxic diagenesis (Gilleaudeau and Kah, 2015). The Atar Group (units I-3, I-4, and I-5) was termed 'Environment III' by Gilleaudeau and Kah (2015), and was suggested to reflect oxic through to dominantly euxinic conditions, which is again supported by our data (Fig. 5). When combined with additional data reported in Scott et al. (2013), the three studies (Fig. 8) generally show more homogeneity in the data for pericratonic environments (Atar Group) relative to epicratonic settings (El Mreïti Group). However, in contrast to this general observation, Unit I-5 of the Atar Group is reported to reflect persistently euxinic conditions in Gilleaudeau and Kah (2015), whereas in our study we only see evidence for oxic through to anoxic ferruginous depositional

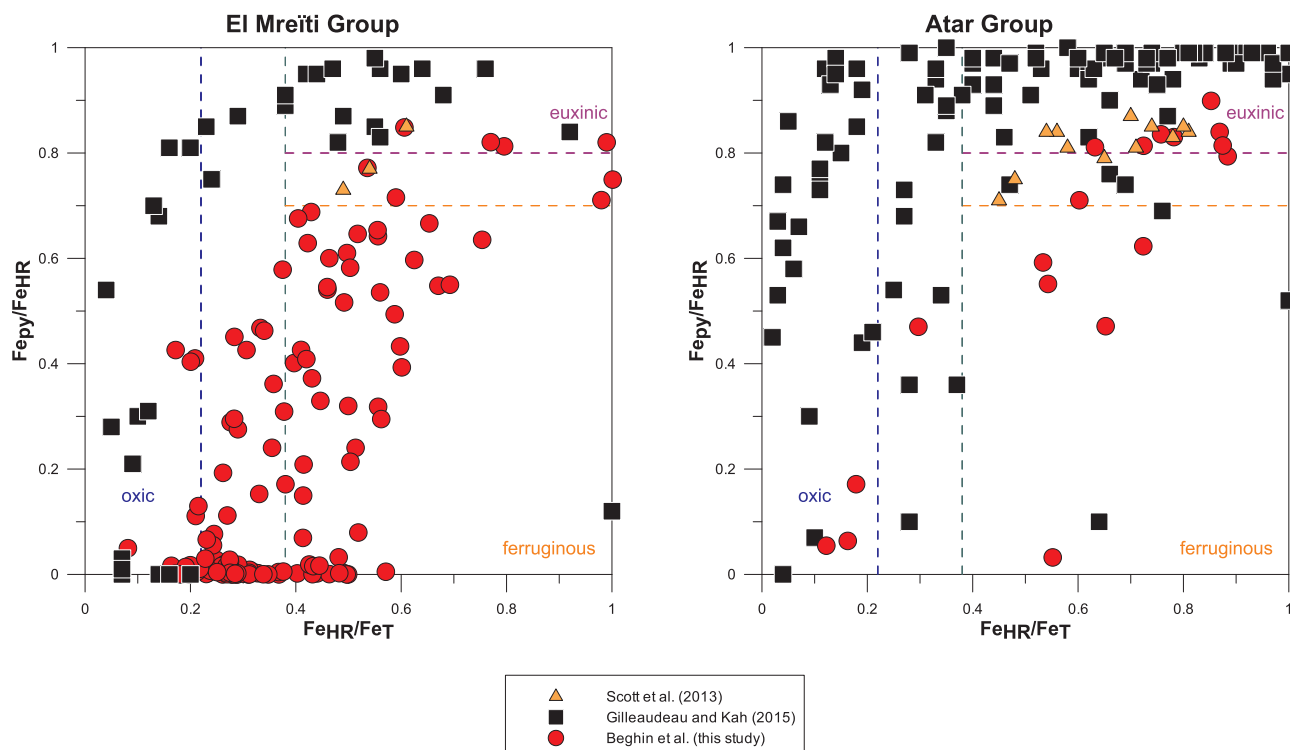


**Fig. 8.** Iron speciation cross plot ( $Fe_{HR}/Fe_T$  and  $Fe_{py}/Fe_{HR}$ ) for all samples from Atar and El Mreïti groups in this study, Scott et al. (2013), and Gilleaudeau and Kah (2015).  $Fe_{HR}/Fe_T \leq 0.22$  = oxic conditions and  $Fe_{HR}/Fe_T \geq 0.38$  = anoxic conditions (vertical dashed lines).  $Fe_{py}/Fe_{HR} \leq 0.8$  or  $\leq 0.7$  = ferruginous conditions and  $Fe_{py}/Fe_{HR} \geq 0.8$  or  $\geq 0.7$  = euxinic conditions (horizontal dashed lines).

conditions (Fig. 5). In previous sedimentological studies, Lahondère et al. (2003) noted that Unit I-5 (Tod) could be coeval with the Tourist and Aguel el Mabha formations (Fig. 2), and Kah et al. (2012) considered Unit I-5 (Atar) as being coeval only with the Tourist Formation. Although stratigraphic correlations based on redox conditions are certainly not robust, we here consider that the studied sediment from Unit I-5 may be coeval to the Aguel el Mabha Formation (both of which show evidence for oxic through to anoxic ferruginous depositional conditions). This is supported by the presence of the species *Trachyhystrichosphaera aimika*, which is observed only within Unit I-5 in the S4 core and in the most proximal environments (Khatt and En Nesoar formations) in the S2 core (Supplementary Table 2). Oxic deeper water would not be expected in an otherwise anoxic stratified restricted basin such as the Taoudeni Basin, where deep water  $O_2$  should be consumed by the organic matter settling through the water column. On the other hand, oxic conditions could originate from local sources such as phototrophic microbial mats (e.g. Riding et al., 2014), but no microbial mats were observed in Unit I-5 and no biomarkers were detected in the S4 core. Nevertheless, while we favour correlation between part of Unit I-5 and the Aguel el Mabha Formation (Lahondère et al., 2003), this remains speculative.

### 5.3. Palaeoecological model for the Atar/El Mreïti Group

Our palaeoecological reconstruction presented in Figs. 9 and 10 considers the distribution of microfossils based on a refined palaeoenvironmental model. In contrast to the model proposed by Gilleaudeau and Kah (2015), we consider marine transgression and regression separately, and consider the studied sediment from Unit I-5 (S4) as coeval to the Aguel el Mabha Formation.

The model also incorporates the biological affinity of the species comprising the Taoudeni microfossil assemblage (Beghin et al., 2017), with the distribution of unambiguous eukaryotes and dominant species of unknown biological affinity (probably prokaryotic *Siphonophycus* spp. and other possibly prokaryotic or eukaryotic) reported

schematically in relation to depositional environment delimited by the white dashed line (species are listed in Supplementary Table 1 with cross-references - identification number (ID n°) - in Supplementary Fig. 1). In Figs. 9 and 10, the horizontal ferruginous zone (background) occurring between oxic and euxinic waters represent the heterogeneity in terms of anoxic episodes, between euxinic and ferruginous conditions. Note that these figures depict a selected view in focusing only on a part of the continental shelf representing the studied material, and not on the whole oceanic basin. For the Fe sources, see Poulton and Canfield (2011).

Epicratonic environments reveal a decrease in the total species richness (S) from shallow-marine tidal-flat (fluvio-deltaic) to marine highstand environments during marine transgression (Fig. 10a). The shallow-marine tidal-flat to subtidal, oxic to intermittently anoxic ferruginous or euxinic, environments preserve a mixed microbial community of both eukaryotes and unknown biological affinities (possibly prokaryotic or eukaryotic). The *incertae sedis* dominate the diversity, both in terms of species richness and abundance (Figs. 6 and 10a). The highest total species richness is observed in the most proximal environment and a peak of eukaryotic relative abundance (mainly process-bearing acritarchs) is observed just before the most extensive flooding of the WAC interior (Figs. 6 and 10a). No unambiguous eukaryotes were observed during the marine highstand in epicratonic environments, characterized by mostly anoxic ferruginous waters and intermittently euxinic (Figs. 9a and 10a). This ecosystem could have been inhabited exclusively by prokaryotes, as suggested by the relatively high abundance of coccoidal colonies (*Eomicrocystis malgica*) and microbial mats with pyritized filamentous sheaths, or alternatively eukaryotes were not preserved (see discussion Section 5.4). However, the biological affinity of *Eomicrocystis malgica* and purported prokaryotic communities inhabiting and producing microbial mats is unknown at this point. In pericratonic environments (persistently anoxic with euxinia more prevalent), a mixed assemblage with a relatively low abundance of eukaryotes is observed (Fig. 10a).

After the marine regression, low species richness and abundance of

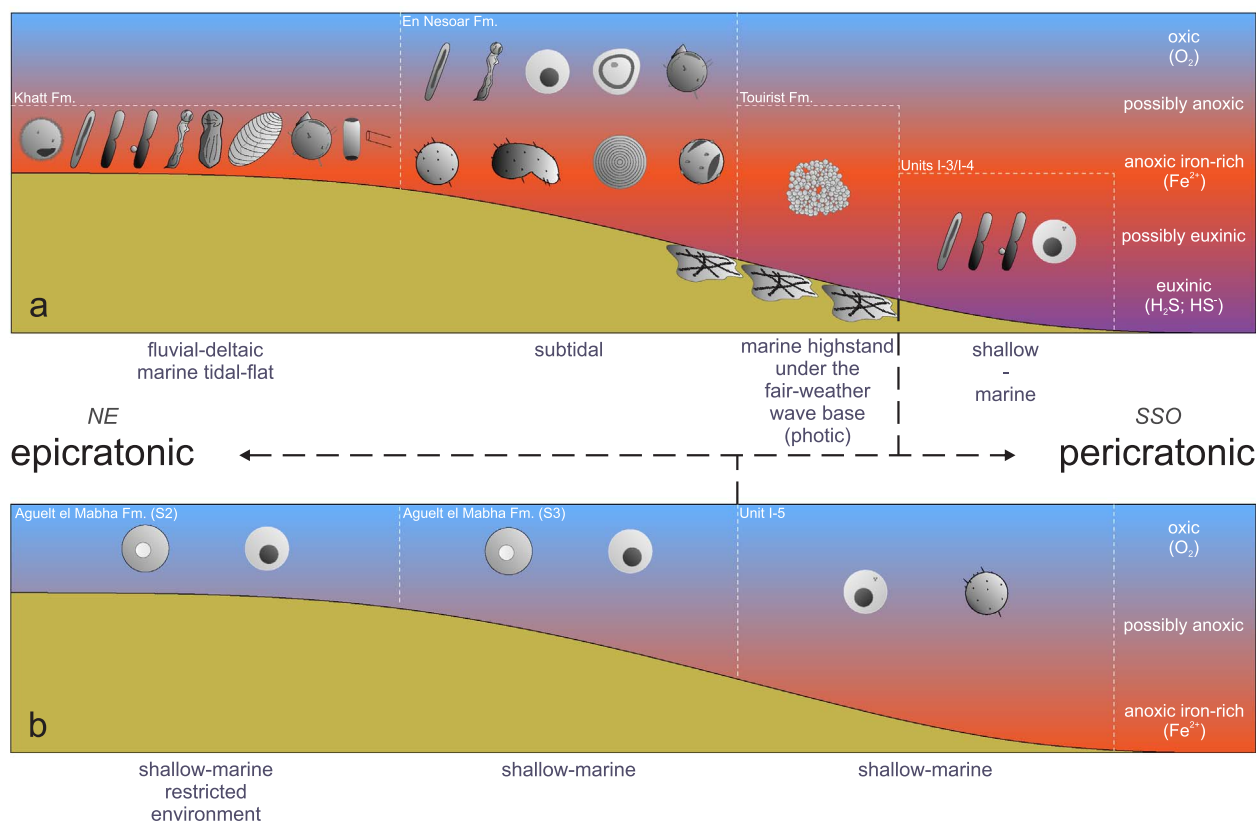


**Fig. 9.** Palaeoecological model for the Atar/El Mreiti Group. Eukaryotic species richness assemblages and notable features in their depositional environments. (a) Marine transgression and (b) marine regression. Notable features are  $\geq 20\%$  (up to 95%) of relative abundance excepted for *Arctacellularia tetragonala* and *Siphonophycus* spp. which are  $\geq 5\%$ . Relative abundance of microfossil specimens is calculated without the total number of microbial mats. Ubiquitous genera such as *Leiosphaeridia* and *Synsphaeridium* are not represented. For the signification of the schematic drawing of the microfossils see [Supplementary Table 1](#) and [Supplementary Fig. 1](#) (ID n°).

eukaryotes are apparent in both epicratonic and pericratonic environments (oxic to anoxic with low sulphide) (Figs. 9b and 10 b).

#### 5.4. Taphonomy and palaeoecology

The preservation of the organic-walled microfossils and microbial mats is exquisite except in the I-3 and I-4 units (core S4). Note that the taphocoenosis (microfossil dead assemblage) is only part of the biocoenosis (the whole living taxonomic diversity). Moreover, fossilization may have occurred at different ontogenetical stages (e.g. vegetative cells, reproductive cysts, dormant bodies in encystment stage).

The oxidation of organic matter, during oxic episodes in shallow-marine restricted environment or during early diagenesis, may have also led to preservation bias and the absence or low abundance of organic-walled microfossils (only very thin-walled and poorly preserved spheroidal vesicles) in the lower Aguel el Mabha from S2 (Figs. 3 and 6), where carbonate-containing shale, lenticular calcareous bodies or planar stromatolites were observed.

Some microfossils observed in the Taoudeni Basin assemblage can most probably be linked to benthic microbial activities (Fig. 10): (1) pyritized filamentous sheaths within amorphous organic matter (microbial mats) found at the base of the En Nesoar and in the Tourist formations (black shale), (2) microbial mats of numerous ( $\geq 5\%$  up to 12%) filamentous sheaths (e.g. *Siphonophycus* spp.), and also maybe (3) *Ostiana microcystis* (sheets of colonial small spheroidal vesicles) mainly found (1–5% of relative abundance) in the Khatt Formation and also to a lesser extent ( $< 0.5\%$ ) in the lower Tourist (S2), the Aguel el Mabha (S3) formations, and in Unit I-5 (S4). These microfossils are mainly of an unknown biological affinity, although *Ostiana microcystis* and *Siphonophycus* spp. are often compared with cyanobacteria (e.g. Butterfield et al., 1994; Javaux and Knoll, 2016). Pyritized filamentous

sheaths within microbial mats could also be linked to primary or secondary sulfur-based metabolism. The other possible eukaryotes and unidentified microfossils (prokaryotes or eukaryotes) could be benthic or planktonic. It is not possible to assess the depth at which the plankton inhabited the water column and thereby their metabolism remains uncertain.

While iron speciation gives an average signal across the sampled sediment interval, biomarkers or fossils might only represent a very short interval within each sample, and thus no conclusion can be drawn regarding possible metabolism based upon our redox proxy data. However, unless benthic microbial mats were very short-lived communities they should have experienced the same average composition of bottom waters during deposition, relative to the sediment. The absence of unambiguous eukaryotes in the Tourist Formation does not appear to be linked to preservation bias or microbial degradation, since smooth-walled sphaeromorphs are preserved within the mats. Gilleaudeau and Kah (2013b, 2015) had noted previously that the presence of a chemocline or a redox interface (below the oxycline and close to euxinia) intersecting the seafloor (Gilleaudeau and Kah, 2015), may have led to a zone of metal sequestration in nearshore settings with extensive drawdown of redox-sensitive trace metals (e.g. Mo, V, and Zn) required for eukaryotic metabolism (Dupont et al., 2006; Havig et al., 2015). The Tourist Formation is characterized by primary productivity driven by microbial mats, leading to high TOC in the sediments (Blumenberg et al., 2012). A possible local depletion in micronutrients close to euxinia may have stimulated the nature of primary production and the apparent dominance of prokaryotes over eukaryotes in the Tourist Formation. Alternatively, eutrophic zones (close to the chemocline) in stratified waters may also lead to a similar ecosystem dominance of prokaryotes over eukaryotes (Butterfield, 2009; Havig et al., 2015).

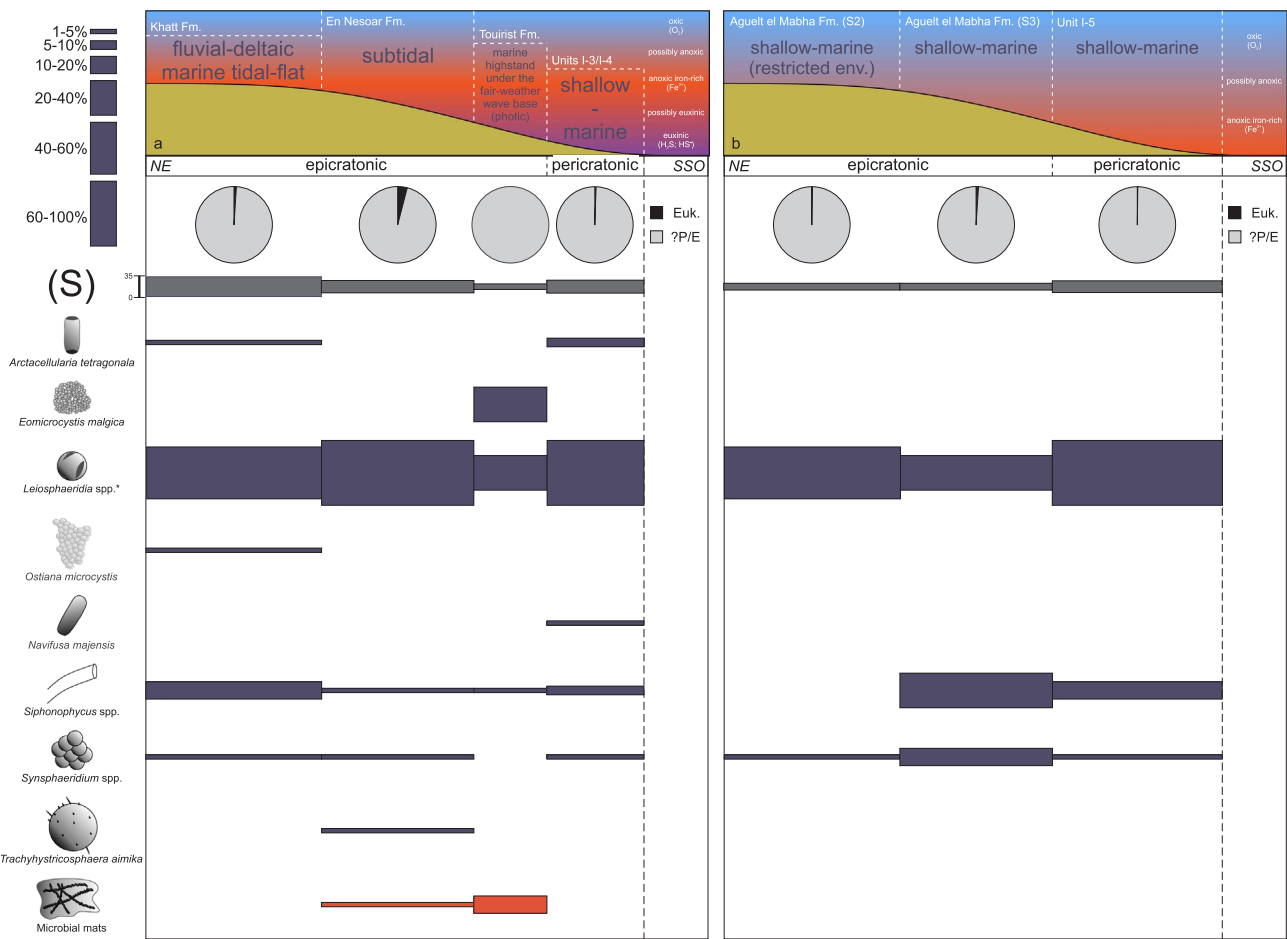


**Fig. 10.** Palaeoecological distribution of the Atar/El Mreiti Group dominant species and features. (a) Marine transgression and (b) marine regression. (S) is species richness. Blue line width is proportional to the species relative abundance (%) calculated for a defined palaeoenvironment (dashed white line): total number of specimens counted for one species/total number of specimens counted within one defined palaeoenvironment). *Leiosphaeridia* spp.\* means all species of the genus *Leiosphaeridia* except *L. kulgunica* and poorly preserved leiospheres. *Spumosina rubiginosa* and *Polytrichoides lineatus* are not represented. Relative abundance of microfossil specimens is calculated without the total number of microbial mats. (For interpretation of the references to colour in this figure legend, the reader is referred to the web version of this article.)

The process-bearing acritarch *Trachyhystrichosphaera aimika* (eukaryotes) is abundant in laminated green-dark-grey shale at the top of the En Nesoar Formation, just before the marine highstand (Tourist Formation). These rocks record anoxic and ferruginous deposition with the exception of one sample recording oxic conditions. In this last sample the relative abundance of *T. aimika* is equal to ~2% while the maximum relative abundance in other En Nesoar samples is equal to ~25%, perhaps reflecting better preservation conditions or ecology. Although *T. aimika* is preserved mainly in rocks deposited under anoxic and iron-rich conditions and mostly in the photic zone of marginal marine environments, it is not possible at this time to evidence its ecological requirements both in terms of light, oxygen, and/or nutrients availability, since its benthic or planktonic habitat and metabolism are unknown.

### 6. Conclusions

The Atar/El Mreiti Group sediments, in the Taoudeni Basin, were deposited in a relatively shallow water environment in pericratonic (western basin) and epicratonic or intracratonic (eastern basin) marine environments during a depositional sequence linked to a marine transgression and regression. Palaeoredox conditions fluctuated from oxic to anoxic states across the basin, but in terms of anoxic episodes, ferruginous conditions dominated in epicratonic environments, while euxinia was more prevalent in pericratonic environments. Oxic conditions were limited and restricted to some horizons in the En Nesoar and

Aguel el Mabha formations, and in Unit I-5. During marine transgression, higher fossil eukaryotic diversity, both in terms of richness and abundance, was observed in more proximal epicratonic environments (oxic to euxinic marginal environments), while no eukaryotes were found in more distal (anoxic ferruginous to euxinic) epicratonic environments represented by marine highstand deposits, and a relatively lower eukaryotic diversity was observed in pericratonic environments (anoxic with euxinia more prevalent). During marine regression, a lower eukaryotic diversity was observed both in epicratonic and pericratonic environments (oxic to anoxic and iron-rich). In agreement to other studies, our palaeoecological model suggests that in the late Mesoproterozoic – early Neoproterozoic, the availability of both molecular oxygen and nutrients controlled and increased eukaryotic diversity in shallow marine marginal environments.

### Acknowledgements

Research support from BELSPO IAP PLANET TOPERS to J. Beghin (PhD scholarship) and E.J. Javaux (PI), and ERC Stg ELiTE FP7/308074 to J.-Y. Storme (postdoc fellowship) and E.J. Javaux (PI) are gratefully acknowledged. J.J. Brocks acknowledges support from the Australian Research Council (DP1095247 and DP160100607). S.W. Poulton acknowledges support from Royal Society Wolfson Research Merit Award. We thank TOTAL S.A. and Jean-Pierre Houzay for access to cores sampling and information and M. Giraldo (ULg) for sample preparation. Reviews by Linda Kah and an anonymous reviewer are greatly

acknowledged.

## Appendix A. Supplementary data

Supplementary data associated with this article can be found, in the online version, at <http://dx.doi.org/10.1016/j.precamres.2017.07.016>.

## References

- Anbar, A.D., Knoll, A.H., 2002. Proterozoic ocean chemistry and evolution: a bioinorganic bridge? *Science* 297, 1137–1142.
- Bartley, J.K., Kah, L.C., 2004. Marine carbon reservoir, Corg-Ccarb coupling, and the evolution of the Proterozoic carbon cycle. *Geology* 32, 129–132.
- Beghin, J., Storme, J.-Y., Blanpied, C., Gueneli, N., Brocks, J.J., Poulton, S.W., Javaux, E.J., 2017. Microfossils from the late Mesoproterozoic – early Neoproterozoic Atar/El Mreïti Group, Taoudeni Basin, Mauritania, northwestern Africa. *Precambrian Res.* 291, 63–82.
- BEICIP, 1981. Nouvelles observations géologiques dans le bassin de Taoudeni. Rapport de la mission de terrain. DMG – DNGM, Paris.
- Benan, C.A.A., Deynoux, M., 1998. Facies analysis and sequence stratigraphy of Neoproterozoic Platform deposits in Adrar of Mauritania, Taoudeni Basin, West Africa. *Geol. Rundsch.* 87, 283–302.
- Bertrand-Sarfati, J., Moussine-Pouchkine, A., 1988. Is cratonic sedimentation consistent with available models? An example from the Upper Proterozoic of the West African craton. *Sediment. Geol.* 58, 255–276.
- Bertrand-Sarfati, J., Moussine-Pouchkine, A., 1992. Formation et comblement d'une dépression intraplatéforme engendrée par la croissance d'un biostrome stromatolitique, Protérozoïque supérieur, Sahara algérien. *C. R. Acad. Sci. (Paris)* 315, 837–843.
- Blumenberg, M., Thiel, V., Riegel, W., Kah, L.C., Reitner, J., 2012. Biomarkers of black shales formed by microbial mats, Late Mesoproterozoic (1.1 Ga) Taoudeni Basin, Mauritania. *Precambrian Res.* 196–197, 113–127.
- Brasier, M.D., Lindsay, J.F., 1998. A billion years of environmental stability and the emergence of eukaryotes: new data from northern Australia. *Geology* 26, 555–558.
- Bronner, G., Rüssel, J., Trompette, R., Clauer, N., 1980. Genesis and geodynamic evolution of the Taoudeni Cratonic Basin (Upper Precambrian and Paleozoic), Western Africa, dynamics of plate interiors. *Am. Geophys. Union* 81–90.
- Buick, R., Des Marais, D.J., Knoll, A.H., 1995. Stable isotopic compositions of carbonates from the Mesoproterozoic Bangemall group, northwestern Australia. *Chem. Geol.* 123, 153–171.
- Buick, R., Knoll, A.H., 1999. Acritarchs and microfossils from the Mesoproterozoic Bangemall Group, northwestern Australia. *J. Paleontol.* 73, 744–764.
- Butterfield, N.J., 2007. Macroevolution and macroecology through deep time. *Palaeontology* 50, 41–55.
- Butterfield, N.J., 2009. Oxygen, animals and oceanic ventilation: an alternative view. *Geobiology* 7, 1–7.
- Butterfield, N.J., 2015. Early evolution of the Eukaryota. *Palaeontology* 58, 5–17.
- Butterfield, N.J., Chandler, F.W., 1992. Palaeoenvironmental distribution of Proterozoic microfossils, with an example from the Agu Bay Formation, Baffin Island. *Palaeontology* 35, 943–957.
- Butterfield, N.J., Knoll, A.H., Swett, K., 1994. Paleobiology of the Neoproterozoic Svanbergfjället formation, Spitsbergen. *Lethaia* 27, 76.
- Canfield, D.E., Raiswell, R., Westrich, J.T., Reaves, C.M., Berner, R.A., 1986. The use of chromium reduction in the analysis of reduced inorganic sulfur in sediments and shales. *Chem. Geol.* 54, 149–155.
- Clarkson, M.O., Poulton, S.W., Guilbaud, R., Wood, R.A., 2014. Assessing the utility of Fe/Al and Fe-speciation to record water column redox conditions in carbonate-rich sediments. *Chem. Geol.* 382, 111–122.
- Clauer, N., 1976. Chimie isotopique du strontium des milieux sédimentaires. Application à la géochronologie de la couverture du craton ouest africain. *Mém. Sci. Géol.* 45, 1–256.
- Clauer, N., 1981. Rb–Sr and K–Ar dating of precambrian clays and glauconies. *Precambrian Res.* 15, 331–352.
- Clauer, N., Caby, R., Jeannette, D., Trompette, R., 1982. Geochronology of sedimentary and metasedimentary precambrian rocks of the West African craton. *Precambrian Res.* 18, 53–71.
- Clauer, N., Deynoux, M., 1987. New information on the probable isotopic age of the late proterozoic glaciation in West Africa. *Precambrian Res.* 37, 89–94.
- Cohen, P.A., Macdonald, F.A., 2015. The proterozoic record of eukaryotes. *Palaeobiology* 41, 610–632.
- Cumming, V.M., Poulton, S.W., Rooney, A.D., Selby, D., 2013. Anoxia in the terrestrial environment during the late Mesoproterozoic. *Geology* 41, 583–586.
- Dupont, C.L., Yang, S., Palenik, B., Bourne, P.E., 2006. Modern proteomes contain putative imprints of ancient shifts in trace metal geochemistry. *Proc. Natl. Acad. Sci. U.S.A.* 103, 17822–17827.
- Evans, D.A.D., 2013. Reconstructing pre-Pangean supercontinents. *Geol. Soc. Am. Bull.* 125, 1735–1751.
- Fenchel, T., 2012. Anaerobic eukaryotes. In: Altenbach, A.V., Bernhard, J.M., Seckbach, J. (Eds.), *Anoxia*. Springer Netherlands, Dordrecht, Heidelberg, London, New York, pp. 5–16.
- Fischer, A.G., 1965. Fossils, early life, and atmospheric history. *Proc. Natl. Acad. Sci. U.S.A.* 53, 1205–1215.
- Gilleaudeau, G.J., Kah, L.C., 2013a. Carbon isotope records in a Mesoproterozoic epicratonic sea: carbon cycling in a low-oxygen world. *Precambrian Res.* 228, 85–101.
- Gilleaudeau, G.J., Kah, L.C., 2013b. Oceanic molybdenum drawdown by epeiric sea expansion in the Mesoproterozoic. *Chem. Geol.* 356, 21–37.
- Gilleaudeau, G.J., Kah, L.C., 2015. Heterogeneous redox conditions and a shallow chemocline in the Mesoproterozoic ocean: evidence from carbon–sulfur–iron relationships. *Precambrian Res.* 257, 94–108.
- Godfrey, L.V., Poulton, S.W., Bebout, G.E., Fralick, P.W., 2013. Stability of the nitrogen cycle during development of sulfidic water in the redox-stratified late Paleoproterozoic Ocean. *Geology* 41, 655–658.
- Guilbaud, R., Poulton, S.W., Butterfield, N.J., Zhu, M., Shields-Zhou, G.A., 2015. A global transition to ferruginous conditions in the early Neoproterozoic oceans. *Nat. Geosci.* 8, 466–470.
- Hallmann, C., Summons, R.E., 2010. Eukaryotes and euxinia before the great oxidation event. *LPI Contrib.* 1538, 5543.
- Havig, J.R., McCormick, M.L., Hamilton, T.L., Kump, L.R., 2015. The behavior of biologically important trace elements across the oxic/euxinic transition of meromictic Fayetteville Green Lake, New York, USA. *Geochim. Cosmochim. Acta* 165, 389–406.
- Jansonius, J., McGregor, D.C., 1996. *Palyngology: Principles and Applications*. American Association of Stratigraphic Palynologists Foundation, Dallas, Texas.
- Javaux, E.J., 2011. Early Eukaryotes in Precambrian Oceans, Origins and Evolution of Life. An Astrobiological Perspective. Cambridge University Presspp. 414–449.
- Javaux, E.J., Knoll, A.H., 2016. Micropaleontology of the lower Mesoproterozoic Roper Group, Australia, and implications for early eukaryotic evolution. *J. Paleontol.* 1–31.
- Javaux, E.J., Knoll, A.H., Walter, M.R., 2001. Morphological and ecological complexity in early eukaryotic ecosystems. *Nature* 412, 66–69.
- Johansson, Å., 2014. From Rodinia to Gondwana with the 'SAMBA' model—a distant view from Baltica towards Amazonia and beyond. *Precambrian Res.* 244, 226–235.
- Johnston, D.T., Wolfe-Simon, F., Pearson, A., Knoll, A.H., 2009. Anoxic photo-synthesis modulated Proterozoic oxygen and sustained Earth's middle age. *Proc. Natl. Acad. Sci. U.S.A.* 106, 16925–16929.
- Kah, L.C., Bartley, J.K., 2011. Protracted oxygenation of the Proterozoic biosphere. *Int. Geol. Rev.* 53, 1424–1442.
- Kah, L.C., Bartley, J.K., Stagner, A.F., 2009. Reinterpreting a Proterozoic Enigma: *Conophyton-Jacutophyton* Stromatolites of the Mesoproterozoic Atar Group, Mauritania, Perspectives in Carbonate Geology. John Wiley & Sons Ltdpp. 277–295.
- Kah, L.C., Bartley, J.K., Teal, D.A., 2012. Chemostratigraphy of the Late Mesoproterozoic Atar Group, Taoudeni Basin, Mauritania: muted isotopic variability, facies correlation, and global isotopic trends. *Precambrian Res.* 200–203, 82–103.
- Kah, L.C., Lyons, T.W., Frank, T.D., 2004. Low marine sulphate and protracted oxygenation of the Proterozoic biosphere. *Nature* 431, 834–838.
- Kah, L.C., Sherman, A.G., Narbonne, G.M., Knoll, A.H., Kaufman, A.J., 1999. 813C stratigraphy of the Proterozoic Bylot Supergroup, Baffin Island, Canada: implications for regional lithostratigraphic correlations. *Can. J. Earth Sci.* 36, 313–332.
- Karlstrom, K.E., Åhäll, K.-I., Harlan, S.S., Williams, M.L., McLelland, J., Geissman, J.W., 2001. Long-lived (1.8–1.0 Ga) convergent orogen in southern Laurentia, its extensions to Australia and Baltica, and implications for refining Rodinia. *Precambrian Res.* 111, 5–30.
- Kendall, B., Reinhard, C.T., Lyons, T.W., Kaufman, A.J., Poulton, S.W., Anbar, A.D., 2010. Pervasive oxygenation along late Archaean ocean margins. *Nat. Geosci.* 3, 647–652.
- Knoll, A.H., 2014. Paleobiological perspectives on early eukaryotic evolution. *Cold Spring Harbor Perspect. Biol.* 6.
- Knoll, A.H., Javaux, E.J., Hewitt, D., Cohen, P., 2006. Eukaryotic organisms in Proterozoic oceans. *Philos. Trans. R. Soc. B: Biol. Sci.* 361, 1023–1038.
- Lahondère, D., Thieblemont, D., Goujou, J.-C., Roger, J., Moussine-Pouchkine, A., LeMetour, J., Cocherie, A., Guerrot, C., 2003. Notice explicative des cartes géologiques et géologiques à 1/200 000 et 1/500 000 du Nord de la Mauritanie Vol. 1 DMG, Ministère des Mines et de l'Industrie, Nouakchott.
- Li, Z.X., Bogdanova, S.V., Collins, A.S., Davidson, A., Waele, B.D., Ernst, R.E., Fitzsimons, I.C.W., Fuck, R.A., Gladkochub, D.P., Jacobs, J., Karlstrom, K.E., Lu, S., Natapov, L.M., Pease, V., Pisarevsky, S.A., Thrane, K., Vernikovsky, V., 2008. Assembly, configuration, and break-up history of Rodinia: a synthesis. *Precambrian Res.* 160, 179–210.
- Lyons, Timothy W., Reinhard, Christopher T., Planavsky, Noah J., 2014. Evolution: a fixed-nitrogen fix in the early ocean? *Curr. Biol.* 24, R276–R278.
- Moore, P.D., Webb, J.A., Collinson, M.E., 1991. *An Illustrated Guide to Pollen Analysis*, second ed. Blackwell Scientific, Oxford.
- Müller, M., Mentel, M., van Hellemond, J.J., Henze, K., Woehle, C., Gould, S.B., Yu, R.-Y., van der Geizen, M., Tielens, A.G.M., Martin, W.F., 2012. Biochemistry and evolution of anaerobic energy metabolism in eukaryotes. *Microbiol. Mol. Biol. Rev.* 76, 444–495.
- Planavsky, N.J., McGoldrick, P., Scott, C.T., Li, C., Reinhard, C.T., Kelly, A.E., Chu, X., Bekker, A., Love, G.D., Lyons, T.W., 2011. Widespread iron-rich conditions in the mid-Proterozoic ocean. *Nature* 477, 448–451.
- Porter, S.M., 2016. Tiny vampires in ancient seas: evidence for predation via perforation in fossils from the 780–740 million-year-old Chuar Group, Grand Canyon, USA. *Proc. R. Soc. Lond. B: Biol. Sci.* 283.
- Poulton, S.W., Canfield, D.E., 2005. Development of a sequential extraction procedure for iron: implications for iron partitioning in continentally derived particulates. *Chem. Geol.* 214, 209–221.
- Poulton, S.W., Canfield, D.E., 2011. Ferruginous conditions: a dominant feature of the ocean through earth's history. *Elements* 7, 107–112.
- Poulton, S.W., Fralick, P.W., Canfield, D.E., 2004. The transition to a sulphidic ocean – 1.84 billion years ago. *Nature* 431, 173–177.
- Poulton, S.W., Fralick, P.W., Canfield, D.E., 2010. Spatial variability in oceanic redox structure 1.8 billion years ago. *Nat. Geosci.* 3, 486–490.

- Poulton, S.W., Raiswell, R., 2002. The low-temperature geochemical cycle of iron: from continental fluxes to marine sediment deposition. *Am. J. Sci.* 302, 774–805.
- Rahmani, A., Goucem, A., Boukhallat, S., Saadallah, N., 2009. Infracambrian petroleum play elements of the NE Taoudenni Basin (Algeria). *Geol. Soc. Lond. Spec. Publ.* 326, 221–229.
- Raiswell, R., Canfield, D.E., 1998. Sources of iron for pyrite formation in marine sediments. *Am. J. Sci.* 298, 219–245.
- Raiswell, R., Newton, R., Wignall, P.B., 2001. An indicator of water-column anoxia: resolution of biofacies variations in the Kimmeridge Clay (Upper Jurassic, U.K.). *J. Sediment. Res.* 71, 286–294.
- Riding, R., Fralick, P., Liang, L., 2014. Identification of an Archean marine oxygen oasis. *Precambrian Res.* 251, 232–237.
- Riedman, L.A., Porter, S.M., Halverson, G.P., Hurtgen, M.T., Junium, C.K., 2014. Organic-walled microfossil assemblages from glacial and interglacial Neoproterozoic units of Australia and Svalbard. *Geology* 42, 1011–1014.
- Roberts, N.M.W., 2013. The boring billion? – lid tectonics, continental growth and environmental change associated with the Columbia supercontinent. *Geosci. Front.* 4, 681–691.
- Rooney, A.D., Selby, D., Houzay, J.-P., Renne, P.R., 2010. Re–Os geochronology of a Mesoproterozoic sedimentary succession, Taoudeni basin, Mauritania: implications for basin-wide correlations and Re–Os organic-rich sediments systematics. *Earth Planet. Sci. Lett.* 289, 486–496.
- Schofield, D.I., Gillespie, M.R., 2007. A tectonic interpretation of “Eburnean terrane” outliers in the Reguibat Shield, Mauritania. *J. Afr. Earth Sc.* 49, 179–186.
- Schofield, D.I., Horstwood, M.S.A., Pitfield, P.E.J., Crowley, Q.G., Wilkinson, A.F., Sidaty, H.C.O., 2006. Timing and kinematics of Eburnean tectonics in the central Reguibat Shield, Mauritania. *J. Geol. Soc.* 163, 549–560.
- Scott, C., Planavsky, N.J., Dupont, C.L., Kendall, B., Gill, B.C., Robbins, L.J., Husband, K.F., Arnold, G.L., Wing, B.A., Poulton, S.W., Bekker, A., Anbar, A.D., Konhauser, K.O., Lyons, T.W., 2013. Bioavailability of zinc in marine systems through time. *Nat. Geosci.* 6, 125–128.
- Stairs, C.W., Leger, M.M., Roger, A.J., 2015. Diversity and origins of anaerobic metabolism in mitochondria and related organelles. *Philos. Trans. R. Soc. B: Biol. Sci.* 370.
- Trompette, R., 1973. Le Précambrien supérieur et le Paléozoïque inférieur de l’Adrar de Mauritanie (bordure occidentale du bassin de Taoudeni, Afrique de l’Ouest). Un exemple de sédimentation de craton. Étude stratigraphique et sédimentologique. *Travaux des Laboratoires des Sciences de la Terre St-Jérôme, Marseille B-7*, 702.
- Trompette, R., Carozzi, A.V., 1994. *Geology of Western Gondwana (2000–500 Ma)*. Balkema, A.A., Rotterdam.
- Verati, C., Bertrand, H., Féraud, G., 2005. The farthest record of the Central Atlantic Magmatic Province into West Africa craton: precise  $^{40}\text{Ar}/^{39}\text{Ar}$  dating and geochemistry of Taoudenni basin intrusives (northern Mali). *Earth Planet. Sci. Lett.* 235, 391–407.
- Villeneuve, M., Cornée, J.J., 1994. Structure, evolution and palaeogeography of the West African craton and bordering belts during the Neoproterozoic. *Precambrian Res.* 69, 307–326.
- Zerkle, A.L., House, C.H., Cox, R.P., Canfield, D.E., 2006. Metal limitation of cyanobacterial  $\text{N}_2$  fixation and implications for the precambrian nitrogen cycle. *Geobiology* 4, 285–297.